ACS Chemical Neuroscience

Research Article

pubs.acs.org/chemneuro

Molecular Determinants of α-Synuclein Mutants' Oligomerization and Membrane Interactions

Igor F. Tsigelny,*[,†,‡,§] Yuriy Sharikov,[†] Valentina L. Kouznetsova,[†,‡] Jerry P. Greenberg,[†] Wolf Wrasidlo,[‡] Cassia Overk,[§] Tania Gonzalez,[§] Margarita Trejo,[§] Brian Spencer,[§] Kori Kosberg,[§] and Eliezer Masliah*[,§,∥]

[†]San Diego Supercomputer Center, [‡]Moores Cancer Center, [§]Department of Neurosciences, and [∥]Department of Pathology, University of California San Diego, La Jolla, California 92093, United States

Supporting Information

ABSTRACT: Parkinson's disease (PD) is associated with the formation of toxic α-synuclein oligomers that can penetrate the cell membrane. Familial forms of PD are caused by the point mutations *A53T*, *A30P*, *E46K*, and *H50Q*. Artificial point mutations *E35K* and *E57K* also increase oligomerization and pore formation. We generated structural conformations of α-synuclein and the above-mentioned mutants using molecular dynamics. We elucidated four main regions in these conformers contacting the membrane and found that the region including residues 39−45 (Zone2) may have maximum membrane penetration. *E57K* mutant had the highest rate of interaction with the membrane, followed by *A53T*, *E46K*, and *E35K* mutants and wild type (wt) α-synuclein. The mutant *A30P* had the smallest percentage of conformers that contact the membrane by Zone 2 than all other mutants and wt α-synuclein. These results were confirmed experimentally in vitro. We identified the key amino acids that can interact with the membrane (Y38, E62, and N65 (first hydrophilic layer); E104, E105, and D115 (second hydrophilic layer), and V15 and V26 (central hydrophobic layer)) and the residues that are involved in the interprotein contacts (L38, V48, V49, Q62, and T64). Understanding the molecular interactions of α-synuclein mutants is important for the design of compounds blocking the formation of toxic oligomers.

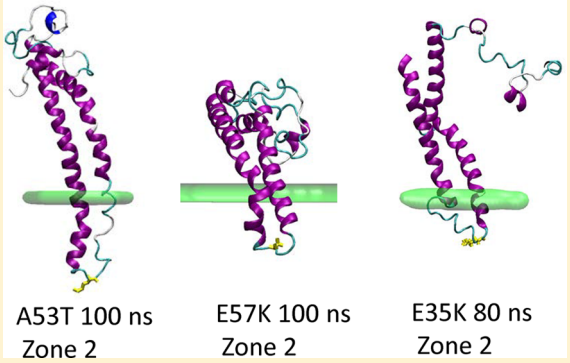

KEYWORDS: *α-Synuclein, α-synuclein mutants, oligomers, neurodegeneration, molecular dynamics, membrane interactions*

Oligomerization of misfolded neuronal proteins and peptides may play a primary role in the pathogenesis of neurodegenerative disorders, including Parkinson's disease (PD), dementia with Lewy bodies, and multiple system atrophy.[1−3] α-Synuclein (αsyn), a neuronal protein of 140 amino acids, accumulates intracellularly in PD, forming oligomeric annular structures and amyloid fibrils, the main components of Lewy bodies. Familial early onset forms of PD are caused by the point mutations *A53T*, *A30P*, *E46K*, *G51D*, and *H50Q*.[4−7] Artificial point mutations *E35K* and *E57K* also show increased oligomerization and toxicity.[8] Biophysical analysis demonstrated that *A30P* and a set of artificial mutants prepared with proline substitutions had reduced αsyn fibrillization propensity but could generate an increased amount of soluble oligomers.[2]

αsyn oligomers interact with the membrane lipids and disrupt the membranes.[2,9−13] Approximately 15% of αsyn molecules are membrane-bound in vivo.[14] Interaction with the membrane for αsyn has been predicted on the basis of sequence analysis and assigned its amphipathic helices containing seven 11-residue repeats as main membrane-contacting regions.[15−17]

Molecular dynamics simulations have been used to simulate the behavior of wild type (wt) αsyn in solution and in a lipid-exposed environment; however, less studies are currently available that model familial and artificial mutants of αsyn. Previous MD simulations of wt and *A30P* mutant αsyn with the truncated C-terminal tail (residues 96−140),[18] have shown nonsignificant loss of helicity at up to 90 ns. Moreover, as shown by surface-sensitive imaging technique, supercritical-angle fluorescence microscopy, and Förster resonance energy transfer,[19] *A53T* and *E57K* mutants damaged the membrane at submicromolar concentrations. *E46K*, *A53T*, and *A30P*/*A53T* αsyn peptides accelerated fibril formation compared with the wt αsyn; on the other hand, *A30P* peptide decelerated fibril formation.[20] The role of *A30P* mutation is not completely clear, because another study with a set of experimental techniques showed the *A30P* mutant was in greater propensity to the membrane than wt αsyn. It was interesting to note that in mouse wt αsyn mutation *A53T* already exists, and does not increase oligomerization.[21] This occurs because other mutations in the wt mouse sequence, especially the mutation *S87N* preventing phosphorylation, compensate for the effect of *A53T* mutation.[22] Extension of the human *A53T* mutant αsyn tertiary

Received: July 3, 2014
Revised: December 30, 2014
Published: January 5, 2015

DOI: 10.1021/cn500332w
ACS Chem. Neurosci. 2015, 6, 403−416

structure (demonstrated by the greater radius of gyration) in comparison with wt αsyn can correlate with the increased protein oligomerization.[22]

Replica exchange molecular dynamics (REMD) studies have been performed with several αsyn mutants. The αsyn mutant *A30P*[23] showed a reduction of its helical propensity for the region 18−31 compared to wt, with an increase of the extension of the tertiary structure of *A30P* mutant vs wt. *E46K* mutant showed some decrease in the average gyration radius of the protein, which agreed with the more compact structure of the protein.[24,25] The αsyn mutant *A53T* showed no significant changes in helicity in the first 100 residues, which is consistent with the NMR studies; however, the more abundant 3_{10}-helix formation was demonstrated for residues V16−A18, E20−T22, E28−E31, V74−V77, and E131−Q134, and the gyration radius for the *A53T* mutant in these MD simulations grew larger than that of wt αsyn.[26] In addition to studies of these mutant αsyn monomers, REMD analysis of 20 ns replicas of possible ensembles of αsyn showed the potential for αsyn to simultaneously form oligomers with high content of α-helices along with oligomers with high β-strand content and unstructured monomers.[27]

MD simulation studies of some of the αsyn mutants have identified conformational changes leading to oligomerization that might be linked to interactions with the membrane; however, the general mechanism leading to increased oligomerization of these mutants is not completely clear. For this reason, we generated by MD multiple structural conformations of αsyn. We showed that there are four main regions that contact the membrane among all the mutants and that the region including residues 39−45 (Zone2) has the maximum membrane penetration. We also showed that the *E57K* mutant had the maximum percentage of conformers contacting the membrane via Zone2 followed by *A53T* and *E46K*, *E35K* mutants, wt αsyn, and *A30P* mutants. We studied the possible ring oligomers formation for all mutants and analyzed their protein−lipids interaction. Based on these results, key amino acids were identified that stabilized the monomers, interacted with the membrane, and involved interprotein contacts within the rings.

RESULTS

Overview of Approach. To study the structural diversity of αsyn mutants and possible annular oligomers, as well as to identify amino acid (aa) residues involved in membrane interactions, we developed a new combined modeling approach (Figure S1, Supporting Information). We generated different structural conformations of αsyn using implicit molecular dynamics (MD) and then examined secondary and tertiary structural changes in conformers along their MD traces. Then we analyzed the membrane interactions of the conformers along their MD traces. We elucidated the main regions of the proteins that interacted with the membrane and calculated percentages for these regions of wt and each mutant αsyn. The conformers of wt and mutant αsyn were then used in attempts to estimate whether they would be able to form the propagating dimers and further annular oligomers using the consecutive docking procedure to evaluate the possibility of quaternary structural formation. As a result, we obtained the annular oligomers that were embedded to the membrane and then underwent MD equilibration in the membrane surrounded by explicit solvent to estimate the stability of the possible transmembrane channels created by wt αsyn and its mutants. Then we analyzed the possible protein−lipid contacts for each ring structure and studied the intermolecular interactions between the neighboring αsyn monomers within the annular oligomers. The general scheme of three-level sets of protein residues interactions made it possible to suggest the points of drug interactions.

αsyn and Its Mutants' Conformational Changes during MD. αsyn and its mutants, as the unstructured proteins, had a number of different conformations (Figure 1).

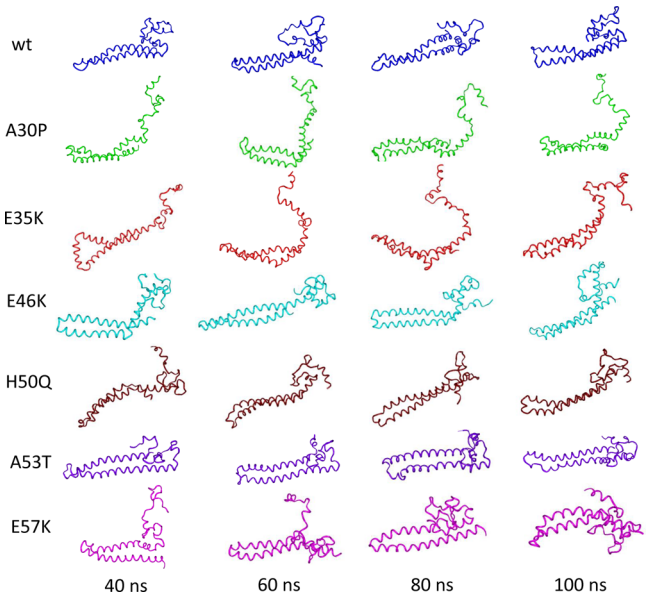

Figure 1. Twenty nanosecond interval MD snapshots of mutants and wt αsyn conformers. The secondary structure of the initial NMR conformation containing a significant percentage of α-helices changes during MD. Additional turns interrupting α-helices appeared on early stages of MD in *E35K* and *E57K* mutants. C-terminal tail became less extended on early stages of MD in wt αsyn and *E46K*, *H50Q*, *A53T*, and *E57K* mutants.

The secondary structure of the initial micelle-bound conformation of αsyn (as in the initial PDB file) did not change significantly during 100 ns of MD in implicit solvent. No extensive unfolding was noticed during the simulation time. That is consistent with the results of 90 ns MD simulation of *A30P* αsyn mutant.[18] At the same time, the helical parts of the conformers underwent some changes during MD. Additional turns interrupting helices appeared in the early stages of MD in *E35K* and *E57K* mutants. C-terminal tail acquired a compact form in the early stages of MD in wt, *E46K*, *H50Q*, *A53T*, and *E57K* mutants. A set of dimers leading to annular oligomers were generated from these initial conformers. Interactions between N-terminal and the middle parts of the protein prevail in forming these dimers (Figure 2). C-terminal tails mostly do not participate in that formation. The α-helical content decreases toward 100 ns of MD, in the *A53T* mutant and increases in all other cases (Figure 3, Supporting Information Figure S2). DSSP analysis shows that in general the α-helical content does not change more than 20% in all cases, which is consistent with the results of Chatterjee and Sengupta.[18] αsyn α-helices are transformed into turns and loops only within specified regions. Wt αsyn is transformed to the set of turn-loop structures in the regions of residues 43−56, 83−87, and 96−99 (Figure 3A). Such a transformation also occurs in the mutants at the region around 39−55 residues, though this

DOI: 10.1021/cn500332w
ACS Chem. Neurosci. 2015, 6, 403−416

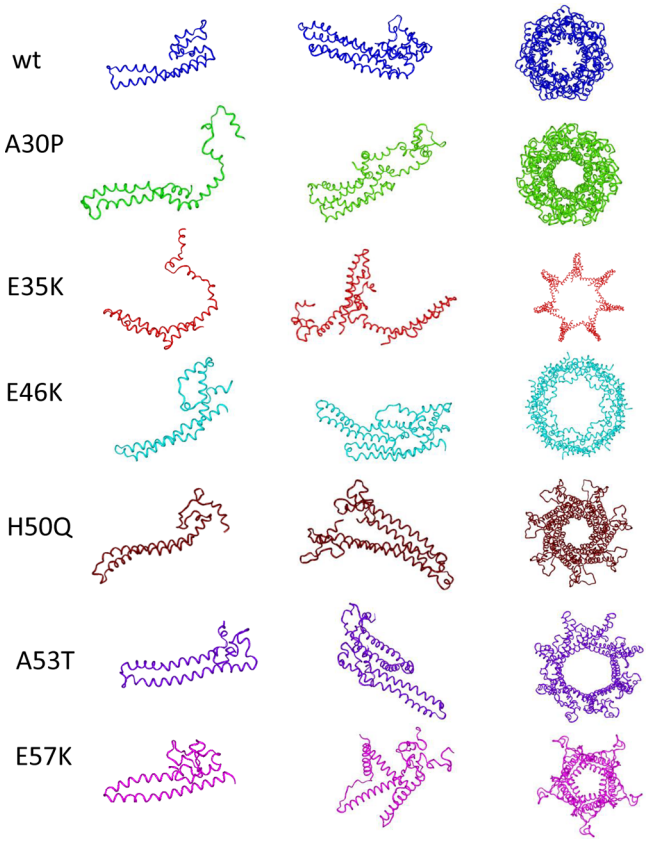

Figure 2. Examples of possible dimers propagating to annular oligomers. These dimers are generated from the initial conformers by selection of the best energy docking positions, consecutive elongation (see Methods section), and MD equilibration in water box. The annular oligomers have from 5 to 7 monomer proteins.

varies for different mutants. For *A30P* mutant (Figure 3B), and more profoundly for *E35K* and *H50Q* mutants (Figure 3C and E), the transformation region shifts toward the region 39−45. For *E46K* mutant, such a shift occurs after around the 50 ns MD point (Figure 3D). Interestingly, these regions correspond to the increased mobility regions found by Perlmutter and coauthors.[28] Moreover, the turn around the region 39−45 has been shown to be the most probable membrane-penetrating zone by Fantini and Yahi[29] for αsyn. Note that during MD new α-helical regions start to appear in the C-terminal part of the protein (Figure 3). In wt αsyn, they appear within the region 110−130 and in the later stage of MD at the region 130−140 (Figure 3A). In *A30P* mutant, they appear in the region 100−130 and also on the later stages of MD in the region 130−140 (Figure 3B). In *E35K* and *E46K* mutants, the α-helices appear almost on the entire length of the C-terminal interrupted by small turns and coils (Figure 3C and D). In *H50Q* mutant, α-helices appear only in the small sections 100−106 and 130−140 (Figure 3E). In *A53T* mutant, most of the relatively long-term new helices appear in the section 130−140 (Figure 3F). In *E57K* mutant, some new α-helices appear on the early stages of MD in the region 100−110 and then disappear, and in the latest stages of MD they appear in the region 130−140.

We conducted the cluster analysis of all MD conformers. This analysis defined the clans including the most represented conformational states during MD runs (Table S1, Supporting Information). The most populated clans' centroids for wt and mutant αsyn molecules were found in the MD times after 50 ns. Other small clans included one or two conformers. Only the centroids of the most populated clans were used for generation of dimers and further oligomers. It is interesting to note that there were no more than four most populated clans of conformers in all mutants and wt protein. These clans' centroids are situated mostly in the second half of the 100 ns runs. For *H50Q* mutant, only one clan has been determined. For each centroid, we created the dimers and checked their possible propagation toward fibrils or rings. The percentage of rings that can be generated from all dimers indirectly corresponds to the possibility of the ring to bind and further penetrate the membrane. Our analysis shows that this parameter in general corresponds to the experimental results (Figure 8E).

Elongation of Conformers and Their Membranephilicity. Starting from the same initial conformation, the mutants and wt conformers had quite different tendencies of elongation. The *E57K* mutant and wt αsyn, closer to 100 ns, had the smaller radii of gyration (R_{gyr}). Maximum R_{gyr} and corresponding elongation showed the *A30P* and *E35K* mutants, followed by *H50Q*, *A53T*, and *E46K* mutants (Figure 4A). The increase in the elongation of conformers during various MD experiments was previously demonstrated for *A30P*[25] and *A53T*[26] mutants; some decrease in elongation was also shown previously for *E46K* mutant conformers.[25] The gyration radii of αsyn and its mutants decreased from around 40 Å at the initial state to between 14 and 30 Å for various mutants.

We calculated membrane-binding propensities of the mutant and wt αsyn MD conformers with a 10 ns interval and elucidated the membrane interactions of these proteins with membranes using our program MAPAS.[30] We discovered that almost all interactions of these proteins with the membrane occur in the four zones of the αsyn sequence (Figure 4B and C). These zones correspond to the regions 2−5 (DVFM), 39−45 (YVGSKTK), 62−67 (QVTNV), and 96−100 (KKDQL) of the αsyn sequence. We called these regions Zone1, Zone2, Zone3, and Zone4, respectively. Membrane binding propensity calculations revealed striking differences in the predicted depths of membrane penetration for different zones. When the predicted membrane penetration for Zones1, 3, and 4 calculated with the program Orientations of Proteins in Membranes (OPM)[31] is around 5 Å (Figures 4D and 5A−H), that means slight immersion to the upper level of the membrane; for Zone2, the program predicted a significantly greater immersion, up to 15 Å (Figures 4D and 5I−N), indicating the possible start of membrane penetration.

Preference for Zone2 in Membrane Contacts of Mutants' Conformers. The program MAPAS[30] selects the best position of a protein on the membrane and calculates the membrane-binding propensity (that we call "membranephilicity") parameters. When we explored each of the snapshot conformers of mutant and wt αsyn, we found that for the wt protein the main membrane-interacting region is Zone1. For all mutants, we observed that the occurrences of the main membrane-penetrating Zone2 increase from 40% in the cases of wt, *E35K*, and *E46K* mutants toward 60% for *A53T* and *E57K* mutant αsyn (Figure 6). The mutant *A30P* shows the lowest percentage of occurrences of Zone2 contacts. Such a result can support a hypothesis that Zone2 can serve as a tip-of-the-membrane penetration process. This result is consistent with the results of Bortolus and coauthors.[32] The increase in the number of conformers having the strongest interactions with the membrane in this region can definitely lead to greater

DOI: 10.1021/cn500332w
ACS Chem. Neurosci. 2015, 6, 403−416

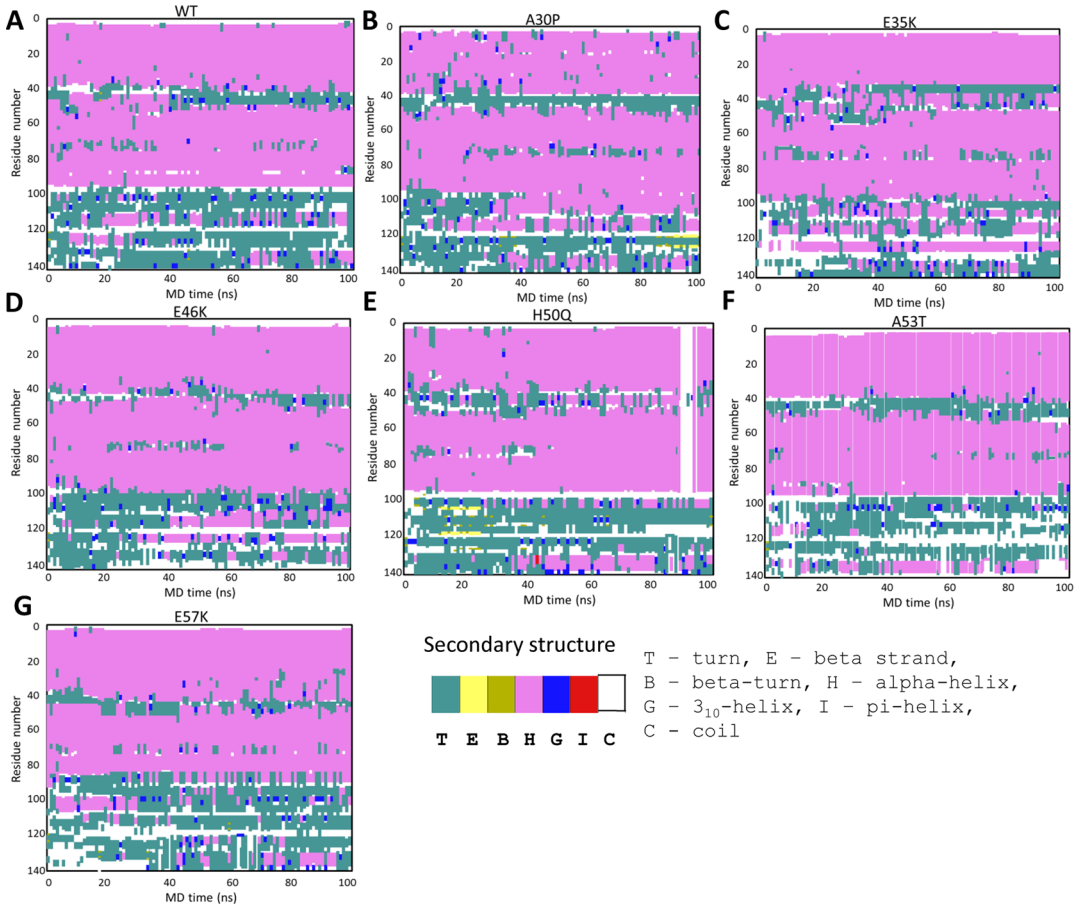

Figure 3. Secondary structure evolution during MD of mutant and wt conformers. wt *α*syn (A) and mutants *A30P* (B), *E35K* (C), *E46K* (D), *H50Q* (E), *A53T* (F), and *E57K* (G). Secondary structure bar: T, turn; E, beta strand, B, *β*-turn; H, *α*-helix; G, 3_{10}-helix; I, *π*-helix; C, coil. The turn-loop secondary structures appear in wt *α*syn at the regions of residues 43−56, 83−87, and 96−99. In *E35K* and *H50Q*, these structures appear at the region 39−45. The new *α*-helical structures start to appear at the C-terminal of the wt and all mutants of *α*syn.

membrane penetration and consistently higher mutant's toxicity. During MD, membranephilicity of all mutants varies, with wt *α*syn showing the lowest values (Figure 6H). Only *A30P* mutant has comparable membranephilicity with wt *α*syn at the last 20 ns of the MD run, which is consistent with the frequency of its Zone2-membrane contacts during MD.

Formation of Membranephilic Conformations in Mutant and wt *α*syns. The conformers of the mutant and wt *α*syns that connect the membrane with the residues of Zone2 have the strongest tendency toward membrane penetration (Figure 6).

The wt *α*syn and *A30P*, *E35K*, and *E46K* mutants show the lowest percentage of the membrane contacts by the Zone2. It increases in the *H50Q*, *A53T*, and *E57K* mutants. Note that such distribution correlates with the experimental gold staining results (Figure 8E).

Table 1 summarizes the contacts that stabilize these conformers. The most frequent contact residues that stabilize the two-helix bundle among all mutant and wt *α*syn conformers are valines 15, 26, and 37 from the N-terminal *α*-helical part and valines 63, 70, and 71 from the central *α*-helical part of the molecules. We analyzed the dynamic of the conformational changes in all of these proteins during MD, trying to understand how the mutations affected the conformational change that shifted the membranephilicity of the mutants.

(1) In wt *α*syn, during MD, there are significantly fewer stabilizing hydrophobic nodes than in the majority of mutants. Note that there are only four such nodes: F4−I88, V15−V71, C29−V55, and the hydrophobic part of K45−V52 (Figure S3A, Supporting Information). Such a limited stabilization network may cause less stable conformation with the membrane-penetrating set of residues at the tip and may permit more conformational changes that would lead to fewer propensities toward membrane penetration.

(2) In *A30P* mutant *α*syn (Figure S3B, Supporting Information), after the first 5 ns, the protein keeps its two-helices structure, with region 39−45 (Zone2) serving as a link/loop between the two helices. Then, at 10 ns, it transforms into the extended conformation that does not have any strong intramolecular contacts. At 20 ns, the mutant evolves into the conformation that shows interactions between the two helices initiated by the mutated P30. This proline became involved in the hydrophobic interaction, with the residue V37 creating a loop that included residues 31−37. Such structural reorganization moves region 26−30 toward region 46−54. The intermediate hydrophobic interaction node appears at 30 ns, between residues P30 and V55. In the next stage, the membranephilic conformation organizational role of P30 ends; finally, at 100 ns, the stabilizing hydrophobic interaction "nodes" appear in the *α*syn conformation (V37−V55, V26−V63, and the hydrophobic part of K21 with P70), and, farther from them, F4 interacts with A85 and I88 (Figure S3B, Supporting Information). This stabilized conformation shows Zone2 in a membranephilic configuration that further leads to

DOI: 10.1021/cn500332w
ACS Chem. Neurosci. 2015, 6, 403−416

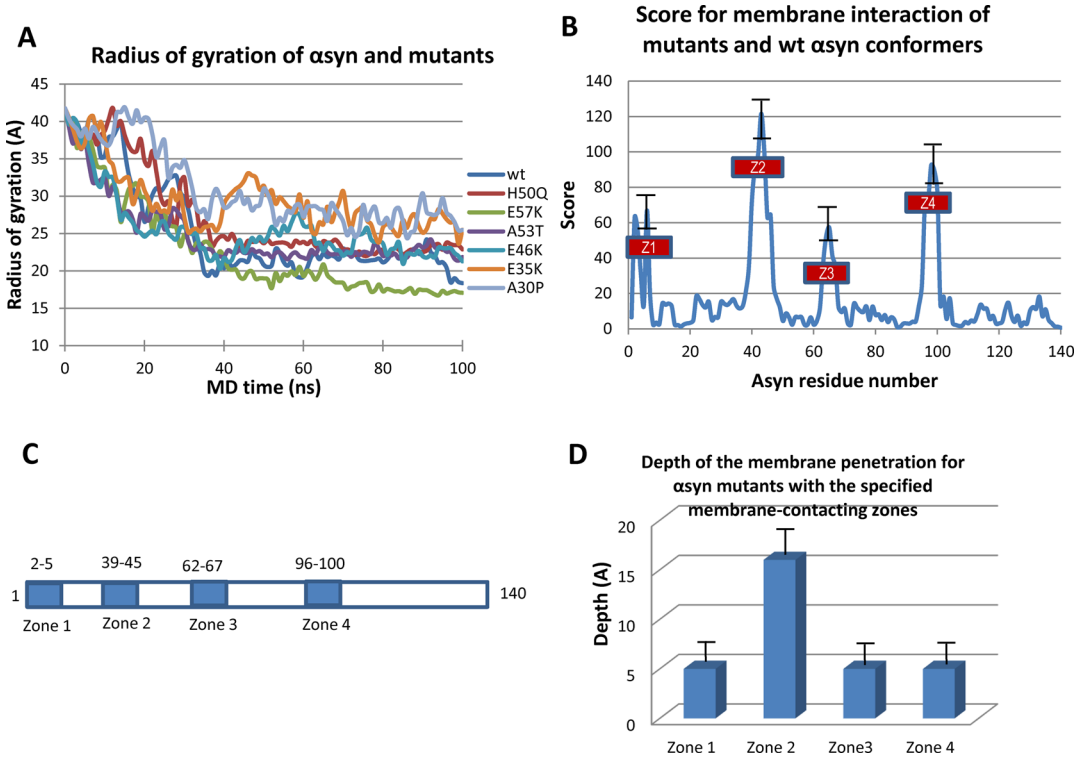

Figure 4. *α*syn tertiary structure evolution and interactions with membrane during MD. (A) Evolution of gyration radii of these proteins during MD. Maximum gyration radii showed the *A30P* and *E35K* mutants, followed by *H50Q*, *A53T*, and *E46K*. (B) Membrane interactions of wt and mutant *α*syn. The majority of interaction with the membrane of all selected with the interval 10 ns wt *α*syn and mutant conformers occurred in the four regions of the wt *α*syn sequence. These regions are located at the residues 2−5, 39−45, 62−67, and 96−100. We called these regions Zone1, Zone2, Zone3, and Zone4. (C) Zones of the greatest membrane interactions for all mutants and wt *α*syn. (D) Depth of membrane penetration of proteins depending on the region of contact. Penetration to around 5 Å means slight immersion to the upper layer of the membrane, For Zone2, we predicted a significantly greater immersion, up to 15 Å, indicating the possible start of the further membrane penetration.

the possibility of deeper membrane penetration and intramembranous ring organization. The residues on the putative penetrating tip of *A30P* mutant are K45 (which has great membranephilicity), V49, and S42.

(3) In *E35K* mutant *α*syn (Figure S3C, Supporting Information), the process of conformation stabilization works differently than in wt *α*syn. In wt *α*syn, negative E35 interacts with neighboring positive K34, keeping the helix in stable conformation. When E35 is mutated into the positive residue *E35K*, a repulsion force appears between K35 and K34 that pushes K34 in another direction until it reaches the first step, stabilizing interaction with the second helix residue, E57. At this stage, the helix is corrupted in region 32−37. The transformation of the helix in this region into a looplike structure leads to the further movement of residues, with stabilization caused by the intrahelix interaction E28−K34. Further, a set of hydrophobic nodes appears: F4−G84, L8−V82, V26−K60, V26−A56, V37−V49, and V40−V48 (Figure S3C, Supporting Information). All these interactions lead to the relatively stable conformation that has a membranephilic loop at Zone2. At the putative membrane-penetrating tip reside the membranephilic residues Y39, S42, T44, K43, and K45.

(4) In *E46K* mutant *α*syn, residues S42, K43, and V49 are situated on the tip of the penetrating conformation. During MD, the conformations-stabilizing hydrophobic interaction nodes F4−A85, F4−I88, K21−V70, V26−V63, and V37−V55 are introduced (Figure S3D, Supporting Information). In the *H50Q* mutant *α*syn, the stabilizing hydrophobic nodes are located closer to N-terminal and the center of the molecule residues: F4−A85, Z11−A78, V15, V71, A18, V70, and only one node close to the putative penetrating tip, V37−V48. *H50Q* exposed V40, T44, K43, K45, and E46 after penetrating Zone2 (Figure S3E, Supporting Information). In the *A53T* mutant *α*syn, we noticed the conformational changes that brought to the tip of the putative membrane-penetration region residue Y39[29] and also the membranephilic K43, H44, E46, and K45. The *A53T* mutant conformation and configuration of the two-helical bundle is heavily stabilized by a set of hydrophobic nodes: F4−V82, the hydrophobic part of K12−V70, V15−V70, V26−V55, V37−V48, V70, and possibly hydrogen bond T22−Q62 (Figure S3F, Supporting Information).

(5) In the *E57K* mutant *α*syn (Figure S3G, Supporting Information), at 10 ns, the *E57K* mutation starts to affect the protein conformational changes. Positive K57 interacts with negative E61, organizing an intermediate salt bridge. The presence of such a bridge strongly changes a possible conformational space. At the second stage (20 ns), a new electrostatic interaction node is formed between E61 and two positive residues, K57 and K58. This interaction helps to bring together the hydrophobic residues V26 and V63, creating the hydrophobic node. Eventually a set of hydrophobic nodes appears. The first is formed by F4 interacting with A85 and I88; the other nodes are formed by A19 and V70, V26 and V63, the hydrophobic part of K32 and A56, V40 and V52, and V37 and V48 (Figure S3G, Supporting Information). On the putative penetrating tip of the *E57K* mutant are membranephilic residues K45 and H50, along with the less membranephilic E46 (similar to wt *α*syn).

DOI: 10.1021/cn500332w
ACS Chem. Neurosci. 2015, 6, 403−416

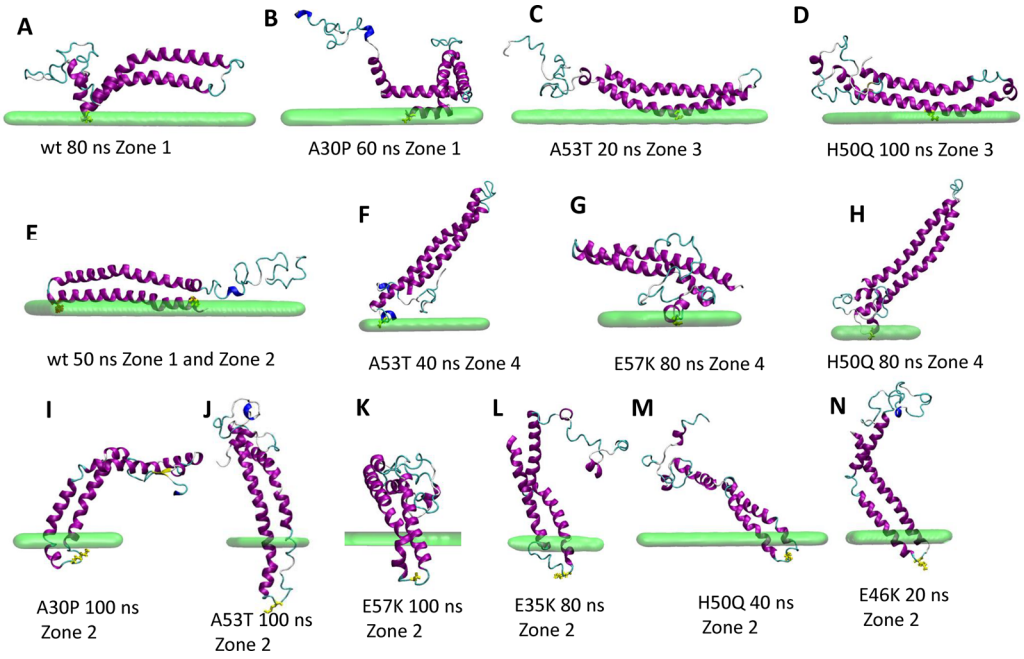

Figure 5. Membrane interaction of mutant and wt αsyn conformers. (A) wt 80 ns conformer contacting the membrane within Zone1. (B) *A30P* mutant 60 ns conformer contacting the membrane within Zone1. (C) *A53T* mutant 20 ns conformer contacting the membrane within Zone3. (D) *H50Q* mutant 100 ns conformer contacting the membrane within Zone3, (E) wt αsyn 50 ns conformer contacting the membrane within both Zone1 and Zone2. (F) *A53T* mutant 40 ns conformer contacting the membrane within Zone4. (G) *E57K* mutant 80 ns conformer contacting the membrane within Zone4. (H) *H50Q* mutant 80 ns conformer contacting the membrane within Zone4. (I) *A30P* mutant 100 ns conformer contacting the membrane within Zone2. (J) *A53T* mutant 100 ns conformer contacting the membrane within Zone2. (K) *E57K* mutant 100 ns conformer contacting the membrane within Zone2. (L) *E35K* mutant 80 ns conformer contacting the membrane within Zone2. (M) *H50Q* mutant 40 ns conformer contacting the membrane within Zone2. (N) *E46K* mutant 20 ns conformer contacting the membrane within Zone2.

Neutralization of Zone2 by Additional Mutants. One of the common features of all conformers presented in Figure S3 (Supporting Information) is the presence of K43 and K45 residues at the tip of Zone2. Positively charged lysine was shown to be one of the residues with the greatest propensity to the cell membranes, which led us to a hypothesis that we could exchange this residue with the residue of an opposite charge or hydrophobic residue. We conducted an in silico experiment, preparing two pairs of additional mutations for all previously described wt and mutant αsyns. The mutations, *K43V* and *K45V* or *K43D* and *K45D*, were added to the already mutated αsyn. We selected *A53T* and *E57K* as the mutants to which these additional mutations (which could abolish Zone2 membrane binding) would have the most notable effect on their interaction with the membrane, since they had the greatest percentage of Zone2 contacts (Figure 7A and B). Additional K43 and K45 mutations strikingly changed the picture of the membrane contact. Actually, no Zone2 contacts remained in any of the K43 and K45 mutants (Figure 7C−F). These results could possibly lead to the design of drugs that would prevent these residues from contacting the membrane.

Generation of Dimers and Oligomers and Selection and Characterization of Oligomeric Rings That Function as Transmembrane Channels. Comparative in vitro biophysical studies[33] demonstrated that acceleration of oligomerization rather than acceleration of fibrillization is a property of αsyn mutants *A53T* and *A30P*. That is why elucidation of possible directions of oligomerization of αsyn and its mutants to annular oligomeric structures is important for understanding of the mechanism of their membrane interactions.

Using the docking program Hex,[34] we constructed dimers for each 10 ns MD conformer for the mutant and wt αsyns. The conformers were docked to their copies, resulting in the generation of distinct dimers. After docking, the dimers underwent the 1.5 ns MD equilibration in the water box. All of the selected dimers showed a stable configuration after equilibration (Figure S4, Supporting Information). These dimers were then expanded through consecutive docking (see Methods section). The obtained dimers undergone 1.5 ns equilibration in water box. Both members of the dimers were reasonably stable after the first ns of equilibration (Figure S5, Supporting Information). Examples of such monomers, dimers, and rings are presented in Figure 2. The oligomers generated from αsyn and its mutants were filtered to identify ring structures that could form transmembrane channels by embedding them to the membrane and MD. Most of the rings created from the most populated clans conformers with the maximum membrane-binding propensity at Zone2 generated stable rings, which were not distorted during the following MD runs (Figure S6, Supporting Information). Energy of interaction of these rings with the membrane sharply stabilizes after the short MD equilibration (Figure S5, Supporting Information).

We studied the membrane lipids' contacts with the protein rings embedded to the membrane (Table 2). If the prediction of the possible transmembrane statuses of such rings is reasonable, these contacts must have a specific pattern. The hydrophilic residues must connect the upper and bottom hydrophilic regions with the heads of lipids, and the hydrophobic residues must contact the hydrophobic lipids region in the middle of the membrane. In the case of *A53T* mutant, residues K80 and D121 contact the top heads-of-lipids

DOI: 10.1021/cn500332w
ACS Chem. Neurosci. 2015, 6, 403−416

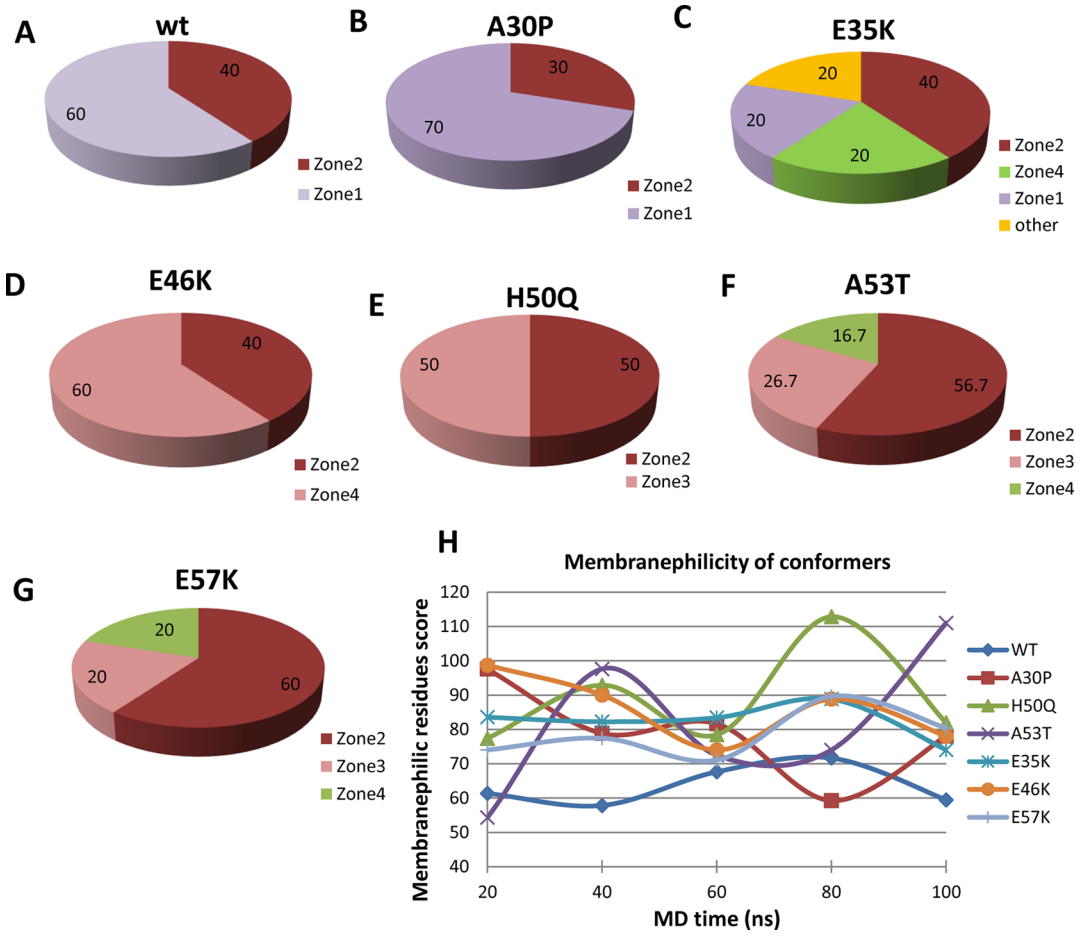

Figure 6. Membrane interactions of wt and mutant αsyn MD conformers. As presented in Figure 4, the main predicted regions of interactions of all wt and mutants conformers with the membrane are Zones1−4. Zone1, residues 2−5; Zone2, residues 39−45; Zone3, residues 62−67; and Zone4, residues 96−100 of the αsyn sequence. Interactions with the membrane differ for various mutants. For all mutants, the occurrences of the main-membrane-penetrating Zone2 increase from 40% in the cases of wt and *E35K* and *E46K* mutants toward 60% for *A53T* and *E57K* mutant αsyn. The mutant *A30P* shows the lowest percentage of occurrences of Zone2 contacts. Such a result can support a hypothesis that Zone2 can serve as a tip-of-the-membrane penetration process. Percentages of these specified regions of the proteins interacting with the membrane during 100 ns MD: (A) wt, (B) *A30P*, (C) *E35K*, (D) *E46K*, (E) *H50Q*, (F) *A53T*, and (G) *E57K*. (H) Membranephilicity of conformers during MD. wt and *A30P* mutant αsyn show the lowest values of the membrane-binding propensity at the last 20 ns of MD which is consistent with the Zone2 contacts prediction of these proteins.

Table 1. Contacts Stabilizing Monomers of wt and Mutant α-Synuclein at 100 ns

	protein						
	wt	*H50Q*	*A30P*	*E35K*	*E57K*	*A53T*	*E46K*
stabilizing contacts	I88−F4	A85−F4	F4−A85	G84−F4	A85−F4	A78−F4	A85−F4
	V71−V15	A78−A11	F4−I88	V82−L8	I88−F4	V82−F4	I88−F4
	V55−A29	V71−V15	V70−K21	A56−V26	V70−A19	V70−K12	V70−K21
	V52−K34	V70−A18	V63−V26	K60−V26	V63−V26	V70−V15	V63−V26
			V55−V37	V49−V37	A56−K32	Q62−T22	V55−V37
				V48−V40	V52−V40	V55−V26	
					V46−V37	V48−V37	

region, V66 and V69 contact the middle hydrophobic part of the bilayer, and the group of T44, E46, and R61 interact with the bottom heads-of-lipids layer. Overall, we see the interacting hydrophobic contacts in the middle of the helices and hydrogen bond interactions on both the top and bottom regions of these helices. The most frequent hydrophilic residues in the top level are Y38, E62, and N65 (first hydrophilic layer); in the bottom level (second hydrophilic layer), E104, E105, and D115; and the most frequent hydrophobic residues interacting with the nonpolar parts of the lipids are V15 and V26 (central hydrophobic layer). In all cases, the H-bond interactions can occur between the ring residues and that both the top and bottom hydrophilic layers of the membrane and hydrophobic residues interact with the central hydrophobic lipid parts at the central part of the membrane.

Interprotein Contacts in the Transmembrane Rings. Table S2 (Supporting Information) shows the interprotein interactions in the membrane-embedded αsyn rings. The

DOI: 10.1021/cn500332w
ACS Chem. Neurosci. 2015, 6, 403−416

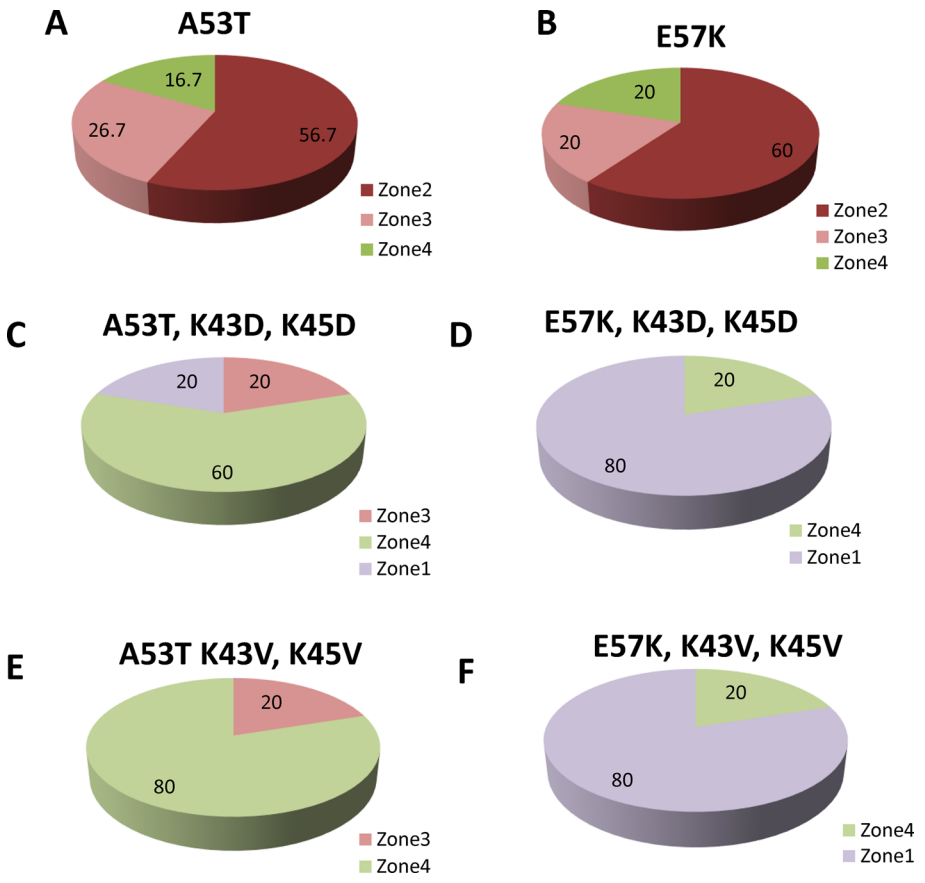

Figure 7. Percentage of conformers contacting the membrane within Zone2 in *A53T* (A) and *E57K* (B) mutants, with the additional mutations *K43D* (C) and *K45D* (D) and *K43V* (E) and *K45V* (F) during MD. Both additional mutations completely eradicate the Zone2 contacts with the membrane. These results predict that substitution of the lysines 43 and 45 in αsyn to either opposite charge residues (aspargic acid) or hydrophobic residue (valine) would completely eradicate the possible Zone2 contacts with the membrane and consistently will significantly inhibit the αsyn membrane penetration.

neighboring monomers in all cases have quite a significant number of ring-stabilizing interprotein interactions. In all cases, these were the combinations of hydrophobic interactions, H-bond, and electrostatic interactions. When for wt αsyn, *H50Q*, and *E57K* mutants interactions between the neighboring monomers in the rings are supported by the combination of hydrophobic, electrostatic forces, and hydrogen bonds, in the other mutants clearly it is seen the bias toward either hydrophobic interactions (*A30P* and *E35K* mutants), or combinations of electrostatic interactions and hydrogen bonds (*E46K*, *A53T*). These results can be taken in consideration in development of strategies for removing of the membrane-embedded αsyn rings.

Immunolocalization of αsyn Mutants to In-Neuronal Cell Membranes. First, the relative levels of αsyn expression between the wt and the mutants were analyzed by immunoblot (Figure 8A). The monomer αsyn band was detected as expected at 14 kDa, with comparable levels of expression between the wt and mutant αsyn. Higher molecular weight bands consistent with dimers, trimers, and higher order oligomers were observed in the wt and mutants, with the *A53T* and *E57K* mutants having the most abundant amount of protein (Figure 8A). Immunocytochemical analysis showed αsyn immunoreactivity in the cytoplasm and around the edges of the neuronal cells infected with LV-control, LV-αsyn wt, and αsyn mutants (Figure 8B). The arrows indicate intensified staining at the edge for the wt, *E46K*, *H50Q*, and *E57K* infected cells, whereas *A30P*-infected cells showed more diffuse staining throughout the cells (Figure 8B). To further determine the subcellular localization of the wt and mutants of αsyn, immunogold and electron microscopy was performed (Figure 8C). These studies showed that gold particles were often found in close proximity to the cell membrane. Gold particles close to the neuronal cell membrane were more abundant in the *H50Q*, *A53T*, and *E57K*-αsyn infected cells and less abundant in the *E46K*, *E35K*, *A30P*, and wt-αsyn infected cells (Figure 8C).

Consistent with our theoretical results, those mutants (*E57K*, *E53T*) that displayed a greater affinity to interact with membranes via Zone2 and therefore a higher propensity to form ring oligomers were the same that showed by electron microscopy a higher concentration of gold particles in the neuronal cell membranes and a greater number of tetrameric oligomers (demonstrated by Western blot) (Figure 8E).

DISCUSSION

Our study showed that increased oligomerization of αsyn mutants might be associated with greater membranephilicity and a propensity to penetrate the membrane. We analyzed snapshots of all mutant and wt αsyn molecules during MD for their propensity to interact with the membrane. Our studies showed that there are four domains within αsyn that mostly contact the membrane, including aa 2−5, 39−45, 62−67, and 96−100, which we denominated Zone1 to Zone4, respectively. We demonstrated that, compared to other domains, the aa

DOI: 10.1021/cn500332w
ACS Chem. Neurosci. 2015, 6, 403−416

Table 2. Contacts of the Embedded Rings with the Membrane

protein	top hydrophilic region	middle hydrophobic region	bottom hydrophilic region
wt	GLU104	hydrophobic part of LYS32	TYR39
	GLU105	VAL55	LYS43
	GLU110		
A30P	GLU114	VAL15	LYS34
	ASP115	VAL26	TYR39
	GLU137	VAL63	
E35K	GLU29	VAL16	ASP2
	LYS35	hydrophobic part of LYS21	LYS6
	HIS50		
E46K	GLU105	ALA76	LYS54
	ASP115	VAL77	GLU61
		hydrophobic part of LYS50	ASN65
H50Q	ASP98	ALA19	GLU57
	GLN99	hydrophobic part of LYS23	LYS60
	GLU104	VAL71	GLU61
			ASN65
A53T	LYS80	ALA63	THR44
	ASP121	VAL66	GLU46
E57K	GLU104	ring of TYR39	HIS50
	GLU105	hydrophobic part of LYS43	
		VAL40	

within Zone2 predicted increased membrane penetration. The presence of defined domains within αsyn molecules that interact with the membrane is consistent with the findings of previous studies[35] that used fluorescent probes and ESR to show that the N-terminal region was the most immersed in the membranes around residue 3 (corresponding to our Zone1), followed by the region around residue 90 (our Zone4), and that the C-terminal was the least immersed. The increased propensity of αsyn Zone2 to penetrate the membrane is consistent with the findings of previous studies[28,29,36] that used mutants *A30P*, *A53T*, and *E46K* in sodium dodecyl sulfate (SDS) detergent micelles and in 1,2-dioleoyl-*sn*-glycero-3-phosphoserine (DOPS) lipid bilayer. Other MD simulations were performed with the explicit solvent method for a maximum of 65 ns for the 1−99 portion of the αsyn.[28] In all these cases, the highest level of protein motion occurs in two regions: the first around 39−45 residues (equivalent to Zone2) and the second around the residues 64−74 (equivalent to Zone3). Moreover, Fantini and Yahi[29] demonstrated, using monolayer experiments with short peptides from the αsyn sequence and MD simulations, that tyrosine 39 insertion through the membrane is a molecular basis for the glycosphingolipid-binding specificity of αsyn and its membrane penetration. The same sphingolipid-binding domain is also common for β-amyloid and prions.[29,37] Di Pasquale and coauthors,[36] using MD and electrophysiological measurements, showed that the major effects of applying the *E46K* mutation were the alteration of the channel properties of αsyn oligomers and the generation of nonstop activity. This mutation is located directly in the region 35−46 (Zone2), which is a bend/loop break between the helices in αsyn and is a main candidate for initiation of the membrane penetration of the protein.

NMR studies[38,39] showed that micelle-bound αsyn contains two α-helical regions: V3−V37 and K45−T92 with unstructured C-terminal tail. The unstructured loop including residues 38−44 (Zone2) links these two helices. A break in the helical structure at region 36−45 (Zone2) of the vesicle-bound αsyn has also been found using NMR.[40] Helix breaks at residues 35−43 (Zone2) were demonstrated using electron spin resonance and MD simulations.[32] Recently, evidence has accumulated regarding the secretion of αsyn in extracellular space and its interaction with specific lipids.[36,41,42] Using the NMR technique, Waudby and coauthors demonstrated that, with the SDS micelles bound to αsyn, the α-helical regions remained mostly stable.[43] Three regions underwent transformations into unstructured loops: 39−45 (Zone2), 63−67 (Zone3), and, to a lesser extent, 83−87 (Zone4). These results correspond to our findings that there are four main zones of contact of αsyn conformers with the membrane, with the Zone2 contacts having significantly greater membrane propensity and penetration. Finally, our results agree with a recent study that used a combination of solid-state and solution NMR spectroscopy to characterize the conformations of αsyn molecules bound to lipid membranes.[44] This study showed three αsyn regions, including an N-terminal helical segment performing the role of membrane anchor, an unstructured C-terminal region that is weakly associated with the membrane, and a central region acting as a sensor of lipid properties and determining the affinity of αsyn membrane binding.[44]

Consistent with our previous studies using wt αsyn,[12,45] we found that αsyn mutants have a greater propensity to interact with and penetrate the membrane through the domain of Zone2 in comparison with the other Zones, that is frequent in the generated conformers with the best energies that form dimers and oligomers. These oligomers have significant interaction with the membrane as they form possibly porelike structures able to lead to outer ions influx and eventual cell death. These oligomers were stable in the membrane because of specific membrane−protein interactions. The oligomer rings interact with the hydrophilic regions in the top of the membrane and organize the H-bonds with the lipid heads. In the middle hydrophobic area of the membrane, the ring proteins interact with the lipids by their hydrophobic residues, while, at the bottom of the membrane, proteins interact with the lipids by their hydrophilic residues. Such an arrangement leads to stable embedding of the rings in the membrane.

Of the various mutations investigated, our study showed that the mutants *E57K* and *A53T* adopted conformations that most frequently favored possible Zone2 interactions with the membrane. *H50Q* is the next in this frequency, and *A30P* is the last. The results of the MD simulation studies are in agreement with our Western blot and immunogold results and are consistent with recent studies[19] showing that *E57K*, followed by *A53T* and wt, has the most interactions with the membrane. Our results are also in agreement with those reported by Ono and coauthors showing that *A30P* has less propensity to interact with the membrane.[20] Analysis of the proximal region of Zone2, the zone that would lead to membrane penetration, showed that, in all cases, K43 and/or K45 were present. We added additional mutations of these two residues to the opposite charge residue−aspargic acid and hydrophobic residue−valine. These mutations led to completely eradicating Zone2 as a possible membrane-contacting region. Our predictions correlate with the experimental

DOI: 10.1021/cn500332w
ACS Chem. Neurosci. 2015, 6, 403−416

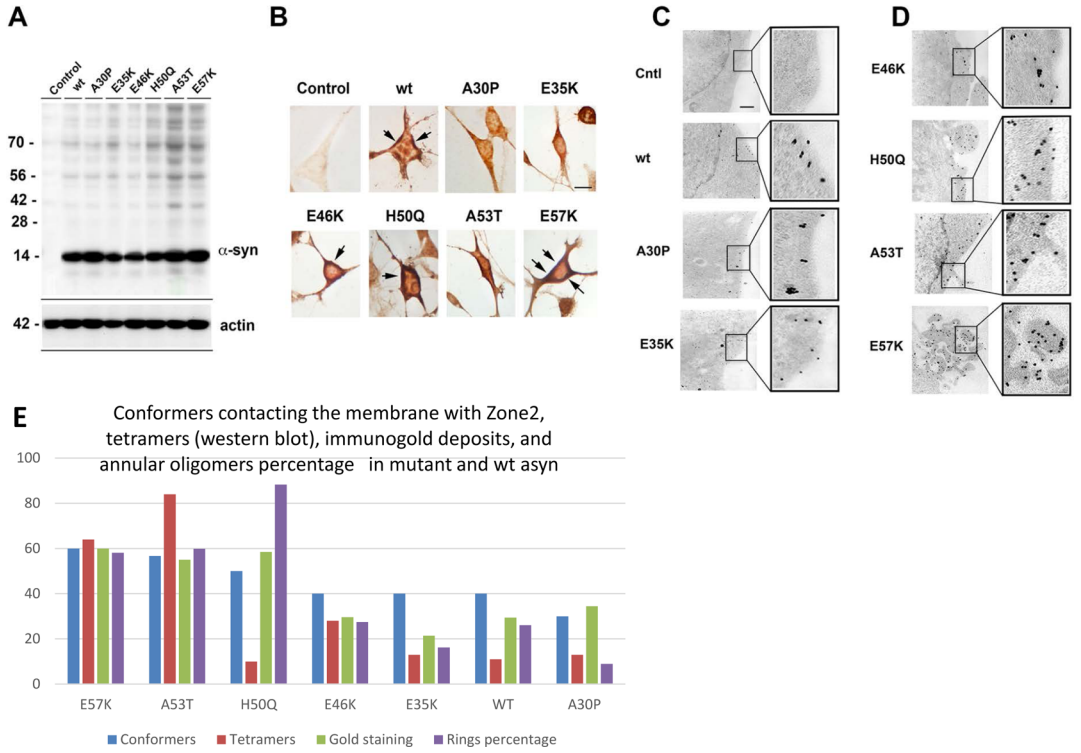

Figure 8. In vitro analysis of αsyn wt and mutant peptides using Western blot, immunocytochemistry, and electron microscopy. (A) Representative Western blot showed the presence of αsyn monomer as well as dimers and oligomers for wt and mutant αsyn with the greatest accumulation of protein for *A53T* and *E57K* αsyn mutations. (B) Immunocytochemistry of B103 cells infected with LC-control and LV-αsyn wt and αsyn mutations. Arrows indicate intensified staining at the edge for wt, *E46K*, *H50Q*, and *E57K* infected cells, whereas *A30P*, *E35K*, and *A53T* infected cells had more diffuse staining throughout the cells. Scale bar = 10 μm. (C) Representative electron micrographs from cells infected with LV-control (Cntl), LV-wt, or LV-αsyn mutants show immunogold deposits associated with the edge of the cells for all LV-αsyn infected cells, which was somewhat increased in E46K infected cells, and (D) greatly increased in *H50Q*, *A53T*, and *E57K* αsyn infected cells. Scale bar = 1 μm. (E) Percentages of conformers contacting the membrane by Zone2 during MD (conformers), western-blot-defined tetramers, and immunogold deposits (gold staining), percentages of ring theoretically formed from the dimers (Ring percentage) for mutant and wt αsyn. The two greatest values for *E57K* and *A53T* are similar for both the theoretical and experimental methods.

results[46] demonstrating that *K45E* mutation of αsyn significantly delays its aggregation.

The general dimensions and number of monomers in the rings predicted by our method correspond to the in vitro experimental results. The porelike annular oligomers with diameters 80−120 Å have been shown using electron microscopy (EM) for wt αsyn[47] and its mutants *A53T* and *A30P*.[48] Analysis of the EM images shows possible numbers of protein monomers 5−7 in these oligomers. Recently cryo-EM images of wt αsyn annular oligomers of with polygon structures including from 3 to 6 monomers and diameter around 100 Å were demonstrated by Zhang and colleagues.[49] Our annular oligomers obtained from αsyn dimers have from 5 to 7 monomers of αsyn. Interesting to note that a percentage of annular oligomers in relation to the total number of dimers for wt and mutant αsyn (one dimer can generate only one oligomer, some of the dimers can generate rings, some generate fibrils, and some do not generate any oligomeric structures) corresponds to our experimental data (Figure 8E). This percentage is higher for *E57K*, *A53T*, and *H50Q* mutants and lower for *E46K*, *E35K*, wt, and *A30P* mutants of αsyn that correlates with the experimental gold staining results.

Further supporting our initial MD results is the fact that the tertiary structures changes reflected in the radii of gyration are consistent with the small-angle X-ray scattering (SAXS) results[50] demonstrated that the gyration radii for wt αsyn and its mutants *A30P*, *E45K*, and *A53T* are between 20 and 42 Å. In our MD simulations for wt asyn and its mutants, radii of gyration are in the range from 14 to 40 Å. In this study, we used the single trajectories of MD for all mutant αsyn. We conducted an additional MD run for 80 ns for wt αsyn. Comparison of conformers from two runs shows that the RMSD difference between the same heavy atoms of the same time snapshots of two runs is not more than 2 Å. We consider the presented MD simulations and other results as a proof of concept. We plan to continue these studies with simulating multiple trajectories for all mutants and wt αsyn.

We therefore concluded that prevention of interactions of αsyn with the membrane might reduce the formation of oligomers and cell toxicity. Our studies suggest four possible points for intervention to abolish the generation of ringlike αsyn oligomers. First, residues that serve in the hydrophobic nodes stabilizing the monomer conformers with the part of Zone2 that interacts with the membrane, here small molecules affecting the conformational evolution of αsyn in solution leading to other, less toxic conformations. Second, our in silico experiments showed that mutations of K43 and K45 may lead to completely eradicating Zone2 contacts with αsyn mutants. Compounds that would bind to this region may prevent the toxic oligomers' formation in the membrane. Third, residues involved in intermolecular interaction in the rings can also serve as points of intervention, here compounds that would have a stable binding to the specific protein regions and serve as the interface inhibitors. Fourth would be the residues of the ring

DOI: 10.1021/cn500332w
ACS Chem. Neurosci. 2015, 6, 403−416

oligomers, which interact with the membrane. This is the most challenging point, because the residues can change their interaction regions depending on the environment. For example, lysines can interact with the hydrophobic regions of lipids with their hydrophobic stems, while the charged region would be stabilized by the neighboring residue of the same or a neighboring protein.

In summary, this study suggests that oligomer-prone αsyn mutants favor conformations that result in the increased interaction of Zone2 with the membrane. Understanding the conformational diversity of αsyn mutants might be important for the rational design of small molecules to block the formation of their toxic oligomers.

METHODS

Molecular Dynamics Simulations of α-Synuclein and Its Mutants. The micelle-bound form of αsyn (PDB ID 1xq8) was used as the initial structure.[38] The structure was mutated into *A53T*, *A30P*, *E46K*, *E35K*, *E57K*, and *H50Q* using the VMD program.[51] We conducted implicit molecular dynamics (MD) for 100 ns using wt αsyn and its mutants as the initial structures, along with the NAMD program (version 2.7).[52] The CHARMM27 force-field parameters[53] were used for MD simulations. The temperature was maintained at 310 K. We used the Generalized Born using Molecular Volume (GBMV) solvent model and Generalized Born Implicit Solvent (GBIS) method. A dielectric constant of water 78.5, intrinsic radius of atoms 0.09 Å, and molar ion concentration 0.15 mol/dm^3 were used. Solvent-accessible surface area (SASA) was calculated using the Linear Combination of Pairwise Overlap (LCPO) method.[54] Surface tension was maintained at 0.005 kcal/mol/Å^2. The alpha cutoff used for calculating Born radius was 15 Å, and nonbonded parameters were cut off at 17 Å. The simulation was performed with initial minimization for 10 000 iterations followed by 0.1° increments heating and equilibrated for 1 ns; then the molecular dynamics simulation was conducted. Data for analysis were taken every 100 ps throughout the simulation. For the water box MD simulations, we used the NAMD 2.6 program with the CHARMM27 forcefield with CMAP correction at the temperature 310 K stabilized using Langevin dynamics and with the fully flexible cell at constant pressure (1 atm) supported by Nosé−Hoover Langevin piston algorithm.[55,56] The studied molecular system had at least 30 Å separation form the box walls. The TIP3P water model was used.

Analysis of Mutant and wt αsyn Conformers. The secondary structures of all MD conformers have been analyzed using the program Define Secondary Structure of Proteins (DSSP).[57] The results were used for elucidation of the specific region in these proteins. Gyration radii were calculated as the parameters related to the protein elongation of all conformers. Membranephilicity parameters for all of them were also measured with our program, MAPAS.[30] The energies of the membrane interactions of these conformers and possible membrane-penetration depths were measured using the Positioning of Proteins in Membranes (PPM) server.[31] Conformers underwent clustering by structural similarity using Shindialov's algorithm[58] with the maximum cutoff Z-scores and minimal RMSD between selected members of the clan. The conformer having the best Z-score along with the smallest summary RMSDs of C-α atoms to the same atoms of other conformers was selected as the centroid and used as a representative of its clan.[59]

Elucidation of the Tertiary Structure Elements Interacting with the Membrane. To address a question of possibly common membrane-contacting regions in the αsyn and mutants, we studied interaction with the membrane of the mutant and wt αsyn conformers for each 10 ns step of their MD traces. Membrane-binding propensities were studied with the programs PPM[31] and MAPAS.[30]

Dimer and Oligomer Construction. The conformers representing the most populated clusters of the 100 ns MD run were used for generation of possible annular oligomers. Using the docking program Hex based on the fast Fourier transform (FFT) method,[34] the selected conformers were docked to the copies of themselves, and the best energy dimers were chosen. After that, we conducted equilibration on each of the obtained dimers in a water box. Such time was sufficient to obtain the stable dimer configurations (Figure S4, Supporting Information). During the first 100 ps of the equilibration, possible close contacts introduced by the rigid body docking are corrected, and during further 1 ns most of the dimers stabilize their conformations and their RMSDs do not change significantly after this time. Then, we consequently docked additional copies of the same conformer (one at a time) to each of these dimers, with docking rotation and translation parameters, as in the equilibrated dimer, to extend the dimers. This procedure used three-dimensional (3D) transformation matrices that were preliminarily calculated for each of the starting dimers. Such procedure has been implemented by Yu and Zheng.[60] This step-by-step extension of the original dimer led to three different possible scenarios. The first scenario unfolded when adding an additional αsyn molecule to the dimer became impossible. We called it "non-propagating dimer." In the second scenario, a dimer could propagate, resulting in the eventual formation of a fibril. In the third scenario, a dimer could be consistently enlarged to form an annular structure ("propagating dimer"). For further studies, we used only the conformers that formed propagating dimers, leading to annular oligomers.

Elucidation of Rings' Stability in the Membrane. We selected the annular oligomers with the maximum membrane-binding propensity, or "membranephilicity." For this, we used the PPM server.[31] This server uses the polarity profile of 1,2-dioleoyl-*sn*-glycero-3-phosphocholine (DOPC) bilayer, determined by neutron and X-ray scattering, and distribution of water in DOPC bilayer, determined by spin-labeling experiments. Then, we embedded the selected rings to the combined membrane containing 30% 1,2-palmitoyl-oleoyl-*sn*-glycero-3-phosphoserine (POPS) and 70% 1,2-palmitoyl-oleoyl-*sn*-glycero-3-phosphocholine (POPC) lipids and conducted 0.8 ns MD equilibration for each ring in the explicit water environment to study their stability. We measured the electrostatic and van der Waals energies of interaction of the embedded oligomers with the membrane. All explored oligomers remained stable in the membrane after this procedure (Figure S5, Supporting Information).

Study of Intermolecular Interactions between the Neighboring Molecules of α-Synuclein in Oligomers. We measured the distances between the heavy atoms of the neighboring monomers of αsyn within the ring formations. We considered the possible hydrophobic interaction when the minimum distance between the centers of heavy atoms of the neighboring amino acid was less than or equal to 4 Å. We considered the possible H-bond interaction if the distance between the centers of bond-creating atoms was equal or less than 3 Å. We considered the possible electrostatic interaction if the distance between the centers of charged heavy atoms was less or equal 4.5 Å.

Construction of Lentiviral Vectors. The LV-wt αsyn was characterized in a previous study.[61] LV-αsyn mutant vectors *A30P*, *E35K*, *E46K*, *H50Q*, *A53T*, and *E57K* αsyn were prepared by site-directed PCR mutagenesis (Agilent Technologies). Lentiviruses were packaged by the transient transfection of the three packaging plasmids and the vector plasmid in 293T cells, as previously described.[62,63]

Neuronal Cell Line Treatments, Lentiviral Vectors. The rat neuroblastoma cell line B103 was used for our in vitro experiments because this cell line displays neuronal features, and we have shown that the pathological features of synucleonopathies emerge when infected with LV-αsyn.[62] B103 cells were plated at 3.5×10^4 cells/well on poly-L-lysine-coated glass coverslips. Cells were allowed to attach for 6 h before being infected with LV-control, LV-wt αsyn, or LV mutant αsyn for 48 h (MOI = 50).

Immunoblot. The levels of LV-wt and LV mutant αsyn were analyzed using B103 cell lysates that were extracted and fractioned into soluble and insoluble fractions by ultracentrifugation.[64] Protein (20 μg/lane) was loaded onto 4−12% SDS/PAGE gels, blotted onto PVDF membranes, and incubated with anti-αsyn (SYN211; 1:1000; Millipore) followed by HRP-tagged secondary antibodies (1:5000; Santa Cruz Biotechnology). Bands were visualized by enhanced

DOI: 10.1021/cn500332w
ACS Chem. Neurosci. 2015, 6, 403−416

chemiluminescence (ECL; PerkinElmer, Boston, MA). β-Actin (1:3000) was the loading control.

Immunocytochemistry. B103 cells were fixed in 4% paraformaldehyde and then immunolabeled with antibodies against αsyn (SYN211, Millipore). Briefly, coverslips were incubated overnight at 4 °C with antibodies against total αsyn (1:500, affinity purified rabbit polyclonal, Millipore),[65] followed by biotin-tagged anti-rabbit IgG1 (1:100, Vector Laboratories, Inc., Burlingame, CA) secondary antibodies, avidin D-HRP (1:200, ABC Elite, Vector), and visualization with diaminobenzidine (DAB). Sections were scanned with a digital Olympus bright field digital microscope (BX41).

Electron Microscopy and Immunogold Analysis. B103 cells infected for 48 h with LV-control, LV-wt αsyn, or LV mutant αsyn were postfixed in 1% glutaraldehyde, treated with osmium tetroxide, embedded in Epon Araldite, and sectioned with an ultramicrotome (Leica, Germany).[65] Sections were mounted on nickel grids, etched, incubated with the αsyn antibody (1:50), and labeled with 10 nm Aurion ImmunoGold particles (1:50, Electron Microscopy Sciences, Fort Washington, PA) with silver enhancement. Electron micrographs (25 000× magnification) were obtained.

Image Processing and Analysis. *Immunoblot Image Quantification.* The immunoblot image was quantified using the program ImageJ, v. 1.46r (National Institute of Health, Bethesda, MD). The obtained image was 205 × 290 pixels with 100 dpi resolution. A rectangular mask with axes 30 × 24 pixels was created. The patches were marked with the mask. The *Set Measurements* menu was used to measure Min and Max Gray Value, Centroid, and Integrated Density. The brightness of each patch was measured and then inverted to correspond to expression.

Electron Micrograph Image Quantification and Particle Analysis. The obtained electron micrographs are 372 × 600 pixels at 300 dpi. To process them, the program ImageJ, v. 1.46r (National Institute of Health, Bethesda, MD), was used. The algorithm includes the following steps: Convert RGB images to 32-bit gray scale images; enhance the image contrast using the *Normalize* function, set to 0.6% of the *Saturated Pixels* value; *Find Edges*, using a Sobel edge detector with 3 × 3 convolution kernels for vertical and horizontal derivatives; set a threshold to increase the minimum threshold value; remove noise, using the *Despeckle* median filter; use the *Remove Outliers* filter; and use *Analyze Particles*, which created a list with a particles count and provided the area and location of each particle.

■ ASSOCIATED CONTENT

Supporting Information

Scheme of studies, calculated data for wt and mutant αsyn conformers and oligomers, and their membrane interactions. This material is available free of charge via the Internet at http://pubs.acs.org.

■ AUTHOR INFORMATION

Corresponding Authors

*Mailing address: Department of Neurosciences, University of California, San Diego, La Jolla, CA 92093-0505. Phone 858-822-0953. Fax 858-534-5117. E-mail: itsigeln@ucsd.edu.

*Mailing address: Department of Neurosciences, University of California, San Diego, La Jolla, CA 92093-0624. Phone 858-534-8992. Fax 858-534-6232. E-mail: emasliah@UCSD.edu.

Author Contributions

I.F.T., Y.S., V.L.K., and J.P.G. developed the models and conducted MD; V.L.K. performed image processing and quantitative analysis of experimental data. W.W., C.O., T.G., M.T., B.S., K.K., and E.M. planned, provided, and conducted experiments. All authors contributed to preparation of the manuscript.

Funding

Funding was provided by NIH Grant AG188440 and Neuropore Therapies Inc. grant to E.M..

Notes

The authors declare no competing financial interest.

■ ACKNOWLEDGMENTS

We are grateful for computational support from the San Diego Supercomputer Center (SDSC) at UCSD.

■ ABBREVIATIONS

3D, three-dimensional; aa, amino acid; DAB, diaminobenzidine; DOPC, 1,2-dioleoyl-*sn*-glycero-3-phosphocholine; DOPS, 1,2-dioleoyl-*sn*-glycero-3-phosphoserine; DSSP, Define Secondary Structure of Proteins (program); ELC, enhanced chemiluminescence; EM, electron microscope; FFT, fast Fourier transform; GBIS, Generalized Born Implicit Solvent (method); GBMV, Generalized Born using Molecular Volume; LV, lentivitus; LCPO, Linear Combination of Pairwise Overlap (method); MAPAS, Membrane-Associated-Proteins Assessment; MD, molecular dynamics; MOI, multiplicity of infection; MSA, Multiple System Atrophy; OPM, Orientations of Proteins in Membranes; PD, Parkinson's disease; POPC, 1,2-palmitoyl-oleoyl-*sn*-glycero-3-phosphocholine; POPS, 1,2-palmitoyl-oleoyl-*sn*-glycero-3-phosphoserine; PPM, Positioning of Proteins in Membranes (WEB server); REMD, Replica Exchange Molecular Dynamics; SASA, solvent-accessible surface area; SAXS, small-angle X-ray scattering; SDS, sodium dodecyl sulfate; wt, wild type; αsyn, α-synuclein

■ REFERENCES

(1) Goedert, M. (2001) Alpha-synuclein and neurodegenerative diseases. *Nat. Rev. Neurosci. 2*, 492−501.

(2) Danzer, K. M., Haasen, D., Karow, A. R., Moussaud, S., Habeck, M., Giese, A., Kretzschmar, H., Hengerer, B., and Kostka, M. J. (2007) Different species of alpha-synuclein oligomers induce calcium influx and seeding. *J. Neurosci. 27*, 9220−9232.

(3) Karpinar, D. P., Balija, M. B., Kügler, S., Opazo, F., Rezaei-Ghaleh, N., Wender, N., Kim, H. Y., Taschenberger, G., Falkenburger, B. H., Heise, H., Kumar, A., Riedel, D., Fichtner, L., Voigt, A., Braus, G. H., Giller, K., Becker, S., Herzig, A., Baldus, M., Jäckle, H., Eimer, S., Schulz, J. B., Griesinger, C., and Zweckstetter, M. (2009) Pre-fibrillar alpha-synuclein variants with impaired beta structure increase neurotoxicity in Parkinson's disease models. *EMBO J. 28*, 3256−3268.

(4) Polymeropoulos, M. H., Higgins, J. J., Golbe, L. I., Johnson, W. G., Ide, S. E., Di Iorio, G., Sanges, G., Stenroos, E. S., Pho, L. T., Schaffer, A. A., Lazzarini, A. M., Nussbaum, R. L., and Duvoisin, R. C. (1996) Mapping of a gene for Parkinson's disease to chromosome 4q21-q23. *Science 274*, 1197−1199.

(5) Zarranz, J. J., Alegre, J., Gómez-Esteban, J. C., Lezcano, E., Ros, R., Ampuero, I., Vidal, L., Hoenicka, J., Rodriguez, O., Atarés, B., Llorens, V., Gomez Tortosa, E., del Ser, T., Muñoz, D. G., and de Yebenes, J. G. (2004) The new mutation, E46K, of alpha-synuclein causes Parkinson and Lewy body dementia. *Ann. Neurol. 55*, 164−173.

(6) Singleton, A. B., Farrer, M., Johnson, J., Singleton, A., Hague, S., Kachergus, J., Hulihan, M., Peuralinna, T., Dutra, A., Nussbaum, R., Lincoln, S., Crawley, A., Hanson, M., Maraganore, D., Adler, C., Cookson, M. R., Muenter, M., Baptista, M., Miller, D., Blancato, J., Hardy, J., and Gwinn-Hardy, K. (2003) Alpha-synuclein locus triplication causes Parkinson's disease. *Science 302*, 841.

(7) Krüger, R., Kuhn, W., Müller, T., Woitalla, D., Graeber, M., Kösel, S., Przuntek, H., Epplen, J. T., Schöls, L., and Riess, O. (1998) A30P mutation in the gene encoding alpha-synuclein in Parkinson's disease. *Nat. Genet. 18*, 106−108.

DOI: 10.1021/cn500332w
ACS Chem. Neurosci. 2015, 6, 403−416

(8) Winner, B., Jappelli, R., Maji, S. K., Desplats, P. A., Boyer, L., Aigner, S., Hetzer, C., Loher, T., Vilar, M., Campioni, S., Tzitzilonis, C., Soragni, A., Jessberger, S., Mira, H., Consiglio, A., Pham, E., Masliah, E., Gage, F. H., and Riek, R. (2011) In vivo demonstration that alpha-synuclein oligomers are toxic. *Proc. Natl. Acad. Sci. U. S. A. 108*, 4194−4199.
(9) Conway, K. A., Harper, J. D., and Lansbury, P. T. (1998) Accelerated in vitro fibril formation by a mutant alpha-synuclein linked to early-onset Parkinson disease. *Nat. Med. 4*, 1318−1320.
(10) Conway, K. A., Harper, J. D., and Lansbury, P. T., Jr. (2000) Fibrils formed in vitro from alpha synuclein and two mutant forms linked to Parkinson's disease are typical amyloid. *Biochemistry 39*, 2552−2563.
(11) Tsigelny, I. F., Crews, L., Desplats, P., Shaked, G. M., Sharikov, Y., Mizuno, H., Spencer, B., Rockenstein, E., Trejo, M., Platoshyn, O., Yuan, J. X., and Masliah, E. (2008) Mechanisms of hybrid oligomer formation in the pathogenesis of combined Alzheimer's and Parkinson's diseases. *PLoS One 3*, e3135.
(12) Tsigelny, I. F., Sharikov, Y., Wrasidlo, W., Gonzalez, T., Desplats, P. A., Crews, L., Spencer, B., and Masliah, E. (2012) Role of α-synuclein penetration into the membrane in the mechanisms of oligomer pore formation. *FEBS J. 279*, 1000−1013.
(13) Caughey, B., and Lansbury, P. T. (2003) Protofibrils, pores, fibrils, and neurodegeneration: Separating the responsible protein aggregates from the innocent bystanders. *Annu. Rev. Neurosci. 26*, 267−298.
(14) Lee, H. J., Choi, C., and Lee, S. J. (2002) Membrane-bound syn has a high aggregation propensity and the ability to seed the aggregation of the cytosolic form. *J. Biol. Chem. 277*, 671−678.
(15) Ferreon, A. C., Gambin, Y., Lemke, E. A., and Deniz, A. A. (2009) Interplay of α-synuclein binding and conformational switching probe by single-molecule fluorescence. *Proc. Natl. Acad. Sci. U. S. A. 106*, 5645−5650.
(16) George, J. M., Jin, H., Woods, W. S., and Clayton, D. F. (1995) Characterization of a novel protein regulated during the critical period for song learning in the zebra finch. *Neuron 15*, 361−372.
(17) Davidson, W. S., Jonas, A., Clayton, D. F., and George, J. M. (1998) Stabilization of alpha-synuclein secondary structure upon binding to synthetic membranes. *J. Biol. Chem. 273*, 9443−9449.
(18) Chatterjee, P., and Sengupta, N. (2012) Effect of the A30P mutation on the structural dynamics of micelle-bound αSynuclein released in water: a molecular dynamics study. *Eur. Biophys. J. 41*, 483−489.
(19) Reynolds, N. P., Soragni, A., Rabe, M., Verdes, D., Liverani, E., Handschin, S., Riek, R., and Seeger, S. (2011) Mechanism of membrane interaction and disruption by α-synuclein. *J. Am. Chem. Soc. . 133*, 19366−19375.
(20) Ono, K., Ikeda, T., Takasaki, J., and Yamada, M. (2011) Familial Parkinson disease mutations influence α-synuclein assembly. *Neurobiol. Dis. 43*, 715−724.
(21) Nielsen, S. B., Macchi, F., Raccosta, S., Langkilde, A. E., Giehm, L., Kyrsting, A., Svane, A. S., Manno, M., Christiansen, G., Nielsen, N. C., Oddershede, L., Vestergaard, B., and Otzen, D. E. (2013) Wildtype and A30P mutant alpha-synuclein form different fibril structures. *PLoS One 8*, e67713.
(22) Losasso, V., Pietropaolo, A., Zannoni, C., Gustincich, S., and Carloni, P. (2011) Structural role of compensatory amino acid replacements in the α-synuclein protein. *Biochemistry 50*, 6994−7001.
(23) Wise-Scira, O., Aloglu, A. K., Dunn, A., Sakallioglu, I. T., and Coskuner, O. (2013) Structures and free energy landscapes of the wild-type and A30P mutant-type α-synuclein proteins with dynamics. *ACS Chem. Neurosci. 4*, 486−497.
(24) Wise-Scira, O., Dunn, A., Aloglu, A. K., Sakallioglu, I. T., and Coskuner, O. (2013) Structures of the E46K mutant-type α-synuclein protein and impact of E46K mutation on the structures of the wild-type α-synuclein protein. *ACS Chem. Neurosci. 4*, 498−508.
(25) Fredenburg, R. A., Rospigliosi, C., Meray, R. K., Kessler, J. C., Lashuel, H. A., Eliezer, D., and Lansbury, P. T. (2007) The impact of the E46K mutation on the properties of alpha-synuclein in its monomeric and oligomeric states. *Biochemistry 46*, 7107−7118.
(26) Coskuner, O., and Wise-Scira, O. (2013) Structures and free energy landscapes of the A53T mutant-type α-synuclein protein and impact of A53T mutation on the structures of the wild-type α-synuclein protein with dynamics. *ACS Chem. Neurosci. 4*, 1101−1113.
(27) Gurry, T., Ullman, O., Fisher, C. K., Perovic, I., Pocharpsky, T., and Stultz, C. M. (2013) The dynamic structure of α-synuclein multimers. *J. Am. Chem. Soc. 135*, 3865−3872.
(28) Perlmutter, J. D., Braun, A. R., and Sachs, J. N. (2009) Curvature dynamics of alpha-synuclein familial Parkinson disease mutants: Molecular simulations of the micelle- and bilayer-bound forms. *J. Biol. Chem. 284*, 7177−7189.
(29) Fantini, J., and Yahi, N. (2011) Molecular basis for the glycosphingolipid-binding specificity of α-synuclein: Key role of tyrosine 39 in membrane insertion. *J. Mol. Biol. 408*, 654−669.
(30) Sharikov, Y., Walker, R. C., Greenberg, J., Kouznetsova, V., Nigam, S. K., Miller, M. A., Masliah, E., and Tsigelny, I. F. (2008) MAPAS: a tool for predicting membrane-contacting protein surfaces. *Nat. Methods 5*, 119.
(31) Lomize, M. A., Pogozheva, I. D., Joo, H., Mosberg, H. I., and Lomize, A. L. (2012) OPM database and PPM web server: resources for positioning of proteins in membranes. *Nucleic Acids Res. 40*, D370−D376.
(32) Bortolus, M., Tombolato, F., Tessari, I., Bisaglia, M., Mammi, S., Bubacco, L., Ferrarini, A., and Maniero, A. L. (2008) Broken helix in vesicle and micelle-bound alpha-synuclein: Insights from site-directed spin labeling-EPR experiments and MD simulations. *J. Am. Chem. Soc. 130*, 6690−6691.
(33) Conway, K. A., Lee, S. J., Rochet, J. C., Ding, T. T., Williamson, R. E., and Lansbury, P. T. (2000) Acceleration of oligomerization, not fibrillization, is a shared property of both alpha-synuclein mutations linked to early-onset Parkinson's disease: implications for pathogenesis and therapy. *Proc. Natl. Acad. Sci. U. S. A. 97*, 571−576.
(34) Macindoe, G., Mavridis, L., Venkatraman, V., Devignes, M. D., and Ritchie, D. W. (2010) HexServer: An FFT-based protein docking server powered by graphics processors. *Nucleic Acids Res. 38* (Web Server issue), W445−W449.
(35) Schvadchak, V. V., Yushchenko, D. A., Pievo, R., and Jovin, T. M. (2011) The mode of α-synuclein binding to membranes depends on lipid composition and lipid to protein ratio. *FEBS Lett. 585*, 3513−3519.
(36) Di Pasquale, E., Fantini, J., Chahihian, H., Meresca, M., Taieb, N., and Yahi, N. (2010) Altered ion channel formation by the Parkinson's-disease-linked E46K mutant of α-synuclein is corrected by GM3 but not by GM1 gangliosides. *J. Mol. Biol. 397*, 202−218.
(37) Mahfoud, N., Garmy, M., Maresca, N., Yahi, A., Puigserver, A., and Fantini, J. (2002) Identification of a common sphingolipid-binding domain in Alzheimer, prion, and HIV-1 proteins. *J. Biol. Chem. 277*, 11292−11296.
(38) Ulmer, T. S., Bax, A., Cole, N. B., and Nussbaum, R. L. (2005) Structure and dynamics of micelle-bound human alpha-synuclein. *J. Biol. Chem. 280*, 9595−9603.
(39) Bisaglia, M., Mammi, S., and Bubacco, L. (2009) Structural insights on physiological functions and pathological effects of alpha-synuclein. *FASEB J. 23*, 329−340.
(40) Drescher, M., Veldhuis, G., van Rooijen, B. D., Milikisyants, S., Subramaniam, V., and Huber, M. (2008) Antiparallel arrangement of the helices of vesicle-bound alpha-synuclein. *J. Am. Chem. Soc. 130*, 7796−7797.
(41) Borghi, R., Marchese, R., Negro, A., Marinelli, L., Forloni, G., Zaccheo, D., Abbruzzese, G., and Tabaton, M. (2000) Full length alpha- synuclein is present in cerebrospinal fluid from Parkinson's disease and normal subjects. *Neurosci. Lett. 287*, 65−67.
(42) El-Agnaf, O. M., Salem, S. A., Paleologou, K. E., Cooper, L. J., Fullwood, N. J., Gibson, M. J., Curran, M. D., Court, J. A., Mann, D. M., Ikeda, S., Cookson, M. R., Hardy, J., and Allsop, D. (2003) Alpha-synuclein implicated in Parkinson's disease is present in extracellular biological fluids, including human plasma. *FASEB J. 17*, 1945−1947.

DOI: 10.1021/cn500332w
ACS Chem. Neurosci. 2015, 6, 403−416

(43) Waudby, C. A., Camilloni, C., Fitzpatrick, A. W., Cabrita, L. D., Dobson, C. M., Vendruscolo, M., and Christodoulou, J. (2013) In-cell NMR characterization of the secondary structure populations of a disordered conformation of α-synuclein within *E. coli* cells. *PLoS One 8*, e72286.
(44) Fusco, G., De Simone, A., Gopinath, T., Vostrikov, V., Vendruscolo, M., Dobson, C. M., and Veglia, G. (2014) Direct observation of the three regions in α-synuclein that determine its membrane-bound behavior. *Nat. Commun. 5*, 3827.
(45) Tsigelny, I. F., Bar-On, P., Sharikov, Y., Crews, L., Hashimoto, M., Miller, M. A., Keller, S. H., Platoshyn, O., Yuan, J. X., and Masliah, E. (2007) Dynamics of alpha-synuclein aggregation and inhibition of pore-like oligomer development by beta-synuclein. *FEBS J. 274*, 1862−1877.
(46) Koo, H. J., Choi, M. Y., and Im, H. (2009) Aggregation-defective alpha-synuclein mutants inhibit the fibrillation of Parkinson's disease-linked alpha-synuclein variants. *Biochem. Biophys. Res. Commun. 386*, 165−169.
(47) Quist, A., Doudevski, I., Lin, H., Azimova, R., Ng, D., Frangione, B., Kagan, B., Ghiso, J., and Lal, R. (2005) *Proc. Natl. Acad. Sci. U. S. A. 102*, 10427−10432.
(48) Lashuel, H. A., Hartley, D., Petre, B. M., Walz, T., and Lansbury, P. T., Jr. (2002) Neurodegenerative disease: amyloid pores from pathogenic mutations. *Nature 418*, 4−5.
(49) Zhang, H., Griggs, A., Rochet, J. C., and Stanciu, L. A. (2013) In vitro study of α-synuclein protofibrils by cryo-EM suggests a Cu^{2+}-dependent aggregation pathway. *Biophys. J. 104*, 2706−2713.
(50) Curtain, C. C., Kirby, N. M., Mertens, H. D., Barnham, K. J., Knott, R. B., Masters, C. L., Cappai, R., Rekas, A., Kenche, V. B., and Ryan, T. (2015) Alpha-synuclein oligomers and fibrils originate in two distinct conformer pools: a small angle X-ray scattering and ensemble optimization modelling study. *Mol. BioSyst. 11*, 190−196.
(51) Humphrey, W., Dalke, A., and Schulten, K. (1996) VMD: Visual molecular dynamics. *J. Mol. Graphics 14*, 33−38.
(52) Kalé, L., Skeel, R., Bhandarkar, M., Brunner, R., Gursoy, A., Krawetz, N., Phillips, J., Shinozaki, A., Varadarajan, K., and Schulten, K. (1999) NAMD2: Greater scalability for parallel molecular dynamics. *J. Comput. Phys. 151*, 283−312.
(53) Feller, S. E., and MacKerell, A. D., Jr. (2000) An improved empirical potential energy function for molecular simulations of phospholipids. *J. Phys. Chem. B 104*, 7510−7515.
(54) Martyna, G. J., Tobias, D. J., and Klein, M. L. (1994) Constant pressure molecular dynamics algorithms. *J. Chem. Phys. 101*, 4177−4189.
(55) Feller, S. E., and MacKerell, A. D., Jr. (2000) An improved empirical potential energy function for molecular simulations of phospholipids. *J. Phys. Chem. B 104*, 7510−7515.
(56) Weiser, J., Shenkin, P. S., and Still, W. C. (1999) Approximate atomic surfaces from linear combinations of pairwise overlaps (LCPO). *J. Comput. Chem. 20*, 217−230.
(57) Kabsch, W. Sander, C. Dictionary of protein secondary structure: Pattern recognition of hydrogen-bonded and geometrical features. *Biopolymers 22*, 2577−2637.
(58) Shindyalov, I. N., and Bourne, P. E. (1998) Protein structure alignment by incremental combinatorial extension (CE) of the optimal path. *Protein Eng. 11*, 739−747.
(59) Tsigelny, I. F., Sharikov, Y., Kouznetsova, V. L., Greenberg, J. P., Wrasidlo, W., Gonzalez, T., Desplats, P., Michael, S. E., Trejo-Morales, M., Overk, C. R., and Masliah, E. (2014) Structural diversity of Alzheimer's disease amyloid-β dimers and their role in oligomerization and fibril formation. *J. Alzheimer's Dis. 39*, 583−600.
(60) Yu, X., and Zheng, J. (2011) Polymorphic structures of Alzheimer's beta-amyloid globulomers. *PloS One 6*, e20575.
(61) Bar-On, P., Crews, L., Koob, A. O., Mizuno, H., Adame, A., Spencer, B., and Masliah, E. (2008) Statins reduce neuronal alpha-synuclein aggregation in in vitro models of Parkinson's disease. *J. Neurochem. 105*, 1656−1667.
(62) Spencer, B., Potkar, R., Trejo, M., Rockenstein, E., Patrick, C., Gindi, R., Adame, A., Wyss-Coray, T., and Masliah, E. (2009) Beclin 1 gene transfer activates autophagy and ameliorates the neurodegenerative pathology in alpha-synuclein models of Parkinson's and Lewy body diseases. *J. Neurosci. 29*, 13578−13588.
(63) Tiscornia, G., Singer, O., and Verma, I. M. (2006) Design and cloning of lentiviral vectors expressing small interfering RNAs. *Nat. Protoc. 1*, 234−240.
(64) Masliah, E., Rockenstein, E., Mante, M., Crews, L., Spencer, B., Adame, A., Patrick, C., Trejo, M., Ubhi, K., Rohn, T. T., Mueller-Steiner, S., Seubert, P., Barbour, R., McConlogue, L., Buttini, M., Games, D., and Schenk, D. (2011) Passive immunization reduces behavioral and neuropathological deficits in an alpha-synuclein transgenic model of Lewy body disease. *PLoS One 6*, e19338.
(65) Masliah, E., Rockenstein, E., Veinbergs, I., Mallory, M., Hashimoto, M., Takeda, A., Sagara, Y., Sisk, A., and Mucke, L. (2000) Dopaminergic loss and inclusion body formation in alpha-synuclein mice: Implications for neurodegenerative disorders. *Science 287*, 1265−1269.

DOI: 10.1021/cn500332w
ACS Chem. Neurosci. 2015, 6, 403−416